

# Supporting Information

Woodhouse et al. 10.1073/pnas.1603351113

In this document, we cover details of statements and derivations in the main text. We first elaborate on the need for a local potential of order higher than quartic, before discussing details of our model: analogies to spin field theories and pure diffusive models, decoupling of loops, and the more active dynamics of a graph of odd degree versus one of even degree. We next show that edges that are equivalent under automorphism obey identical waiting time distributions, we compute the energy barriers for the 3-cycle/4-cycle transitions in  $K_4$ , and we detail the derivation of the cycle basis representation for  $P_{4,1}$  in the incompressible limit. Finally, we consider the use of  $e$ -girth distributions to predict the behavior of active flows on complex networks. We also provide details on numerical methods used throughout this work.

In addition to figures referenced in the following text, we also provide two further figures: Fig. S4, which supplements Fig. 3 by illustrating all 20 asymmetric cubic graphs considered; and Fig. S5, which shows an example integration of totally incompressible flow on a  $15 \times 15$  hexagonal lattice to supplement the discussion of face cycle basis representations.

## SI Local Potential

The typical symmetric, bistable potential is the quartic  $V_4(\phi) = -(1/2)\phi^2 + (1/4)\phi^4$ . However, we use the sixth-order form  $V_6(\phi) = -(1/4)\phi^4 + (1/6)\phi^6$ . This is to force the energy to have discrete local minima once the soft incompressibility constraint is added; we will explain this further here.

Consider the elementary (although not simple!) two-vertex, three-edge graph in Fig. S1A. This has energy

$$H(\phi_1, \phi_2, \phi_3) = \lambda[V(\phi_1) + V(\phi_2) + V(\phi_3)] + \mu(\phi_1 + \phi_2 + \phi_3)^2.$$

In the limit  $\mu/\lambda \gg 1$ , the flow is incompressible, so we can substitute  $\phi_3 = -\phi_1 - \phi_2$  to obtain a reduced energy  $\hat{H}(\phi_1, \phi_2) = \lambda\mathcal{H}(\phi_1, \phi_2)$ , where, assuming a symmetric potential  $V(\phi)$ ,

$$\mathcal{H}(\phi_1, \phi_2) = V(\phi_1) + V(\phi_2) + V(\phi_1 + \phi_2).$$

Local minima of  $\mathcal{H}$  then yield metastable states of the system, independent of  $\lambda$ .

Consider the case  $V = V_4$ . Then  $\mathcal{H}$  factorizes as

$$\mathcal{H} = \frac{1}{2}f(\phi_1, \phi_2)[f(\phi_1, \phi_2) - 2],$$

where  $f(\phi_1, \phi_2) = \phi_1^2 + \phi_1\phi_2 + \phi_2^2$ . Thus,  $\nabla\mathcal{H} = 0$  implies  $(f - 1)\nabla f = 0$ , so either  $f = 1$  or  $\phi_1 = \phi_2 = 0$ . The latter is a local maximum, so our minima are the solutions of  $\phi_1^2 + \phi_1\phi_2 + \phi_2^2 = 1$ . However, this is an ellipse in the  $(\phi_1, \phi_2)$  plane, implying a continuous  $U(1)$ -symmetric set of fixed points. In other words, with  $V = V_4$ , mixed states such as  $(1/\sqrt{3}, 1/\sqrt{3}, -2/\sqrt{3})$  are equally preferable to unit flux states like  $(1, 0, -1)$ . In contrast, the choice  $V = V_6$  results in minima of  $\mathcal{H}$  only at the six states  $(\phi_1, \phi_2) = (\pm 1, 0), (0, \pm 1), (\pm 1, \mp 1)$ , which is the phenomenology we are interested in.

## SI Model

**Relationship to Lattice Spin Field Theory.** Our energy in Eq. 1 can be seen as a generalization of a lattice spin field theory. Suppose we switch to a typical vertex-based picture, where fluxes  $\phi_e$  on edges  $e$  in  $\Gamma$  are now spins  $\psi_i$  on vertices  $i$  in an interaction graph  $\Xi$ . A scalar lattice spin theory then has Hamiltonian

$$H_{\text{spin}} = \lambda \sum_i V(\psi_i) + \frac{1}{2} \mu \sum_{\{i,j\}} (\psi_i \pm_{ij} \psi_j)^2, \quad [\text{S1}]$$

where, in the sum over adjacent spins  $\{i, j\}$  in  $\Xi$ , the sign  $\pm_{ij}$  is  $+$  or  $-$  according to whether the interaction between  $i$  and  $j$  is antiferromagnetic or ferromagnetic, respectively. In our theory, however, multiple spins are permitted inside each interaction term according to the degree of each vertex in  $\Gamma$ . For instance, on a cubic graph, Eq. 1 is equivalent to

$$H = \lambda \sum_i V(\psi_i) + \frac{1}{2} \mu \sum_{\{i,j,k\}} (\psi_i \pm_{ij} \psi_j \pm_{jk} \psi_k)^2,$$

where the interaction is now a sum over interacting triples of spins, one term for each vertex in  $\Gamma$ , with pairwise signs being  $-$  or  $+$  according to whether the corresponding edges in  $\hat{\Gamma}$  are oriented head-to-tail or not at the vertex. Thus, we have essentially defined a theory on an interaction hypergraph  $\Xi$ , with Eq. S1 being the special case where  $\Xi$  is a graph: although Eq. S1 has two types of interaction edge—antiferromagnetic and ferromagnetic—between two spins, the general theory has  $2^{n-1}$  types of interaction hyper-edge between  $n$  spins for all  $n \geq 1$ .

**Diffusive Dynamics When  $\lambda = 0$ .** In the absence of a local edge potential (i.e.,  $\lambda = 0$ ), Eq. 2 reduces to noisy scalar diffusion on the edges of  $\Gamma$ . This process results in a long-term state dominated by a weighted sum of cycles of the graph, as we now describe.

As in the derivation of the incompressible limit (see *SI Incompressible Limit* and *Incompressible Limit*), by analogy with a spectral decomposition for the diffusion equation, we decompose  $\Phi$  into a sum  $\Phi = f_j \Psi^j$  over an orthonormal eigenbasis  $\Psi^j$  of the edge Laplacian  $\mathbf{D}^T \mathbf{D}$ , where  $\Psi^j = (\psi_e^j)$  has eigenvalue  $\nu_j \geq 0$ . The components  $f_i$  then obey

$$df_i = -\mu \nu_i f_i dt + \sqrt{2\beta^{-1}} dW_{i,t},$$

after setting  $\lambda = 0$  and combining independent noise terms. Thus, modes with  $\nu_i > 0$  are damped by the diffusivity  $\mu$  whereas modes with  $\nu_i = 0$  are only subject to noise-induced fluctuations. The non-zero modes' amplitudes follow Ornstein–Uhlenbeck processes and therefore have mean zero and variance  $(\beta\mu)^{-1}$  as  $t \rightarrow \infty$ , whereas, because of the absence of damping, the zero modes' amplitudes follow simple Brownian processes and so have variance  $2\beta^{-1}t$ .

**Decoupling of Loops.** We show here that if  $\Gamma$  contains loops, then these will decouple from the dynamics of the rest of  $\Gamma$ . Consider a loop edge  $\ell \in \mathcal{E}$  incident to a vertex  $w \in \mathcal{V}$ . Then  $\mathbf{D}$  is defined such that  $D_{w\ell} = 0$  (consistent with  $\phi_\ell$  contributing zero to the net flux at  $w$ , because flow in along  $\ell$  always equals flow out along  $\ell$ ). Therefore, using summation convention,  $D_{ve}\phi_e$  is independent of  $\phi_\ell$  for all  $v \in \mathcal{V}$ , which implies  $\partial H / \partial \phi_e$  is independent of  $\phi_\ell$  for all  $e \neq \ell$ , and thus  $\phi_\ell$  decouples. Furthermore,  $(\mathbf{D}^T \mathbf{D}\Phi)_\ell = D_{v\ell} D_{ve} \phi_e = 0$ , so  $d\phi_\ell = -\lambda V'(\phi_\ell) dt + \sqrt{2\beta^{-1}} dW_{\ell,t}$ , meaning  $\phi_\ell$  behaves as a non-interacting Brownian particle in the potential  $V(\phi_\ell)$ .

**Odd- Versus Even-Degree Vertices.** Graphs with odd-degree vertices exhibit more active stochastic cycle selection dynamics than those with even-degree vertices. This is exemplified by the small graphs in Fig. S1, where adding an extra edge markedly slows transition rates. For the graph in Fig. S1A to change state while conserving flux, one edge changes from  $+1$  (or  $-1$ ) to 0

while another simultaneously goes from 0 to  $-1$  (or  $+1$ ), which has an energy barrier  $11\lambda/192$ . However, for the graph in Fig. S1B, one edge changes from  $+1$  to  $-1$  while another goes from  $-1$  to  $+1$ , with an energy barrier  $\lambda/6$  nearly 3 times that of Fig. S1A.

### SI Automorphic Equivalence

In this section, we show that edges within an automorphism equivalence class obey identical waiting time distributions. As in the main text, we assume that  $\Gamma$  does not contain any loops but do allow multiple edges between distinct vertices. In addition, for clarity, we do not use summation convention.

To permit multiple edges, we define an automorphism  $\sigma \in \text{Aut}(\Gamma)$  as a permutation of  $\mathcal{V} \cup \mathcal{E}$  preserving  $\mathcal{V}$  and  $\mathcal{E}$  such that  $v \in \mathcal{V}$  and  $e \in \mathcal{E}$  are incident if and only if  $\sigma(v)$  and  $\sigma(e)$  are incident. Suppose we have flow  $\Phi$  on  $\Gamma$  obeying Eq. 2, whose components read

$$d\phi_e = -\lambda V'(\phi_e)dt - \mu \sum_{v \in \mathcal{V}} \sum_{f \in \mathcal{E}} D_{ve} D_{vf} \phi_f dt + \sqrt{2\beta^{-1}} dW_{e,t}. \quad [\text{S2}]$$

Let  $\Phi^\sigma = (\phi_e^\sigma)$  be the flow vector after permuting by  $\sigma$ , so that  $\phi_e^\sigma = \phi_{\sigma(e)}$ . Replacing  $e$  with  $\sigma(e)$  in Eq. S2 and substituting this definition implies

$$d\phi_e^\sigma = -\lambda V'(\phi_e^\sigma)dt - \mu \sum_{v \in \mathcal{V}} \sum_{f \in \mathcal{E}} D_{v\sigma(e)} D_{vf} \phi_f dt + \sqrt{2\beta^{-1}} dW_{\sigma(e),t}. \quad [\text{S3}]$$

Because  $\sigma$  is a permutation, we can reorder the sums as

$$\sum_{v \in \mathcal{V}} \sum_{f \in \mathcal{E}} D_{v\sigma(e)} D_{vf} \phi_f = \sum_{v \in \mathcal{V}} \sum_{f \in \mathcal{E}} D_{\sigma(v)\sigma(e)} D_{\sigma(v)\sigma(f)} \phi_{\sigma(f)}.$$

Furthermore, because  $\sigma$  preserves incidence but not necessarily orientation,  $D_{\sigma(v)\sigma(e)} = s_e D_{ve}$ , where  $s_e = \pm 1$  according to whether the orientation of  $\sigma(e)$  with respect to  $\sigma(v)$  is the same as or opposite to the orientation of  $e$  with respect to  $v$ . Therefore, Eq. S3 becomes

$$d\phi_e^\sigma = -\lambda V'(\phi_e^\sigma)dt - \mu s_e \sum_{v \in \mathcal{V}} \sum_{f \in \mathcal{E}} D_{ve} D_{vf} \phi_f dt + \sqrt{2\beta^{-1}} dW_{\sigma(e),t}. \quad [\text{S4}]$$

Let  $\tilde{\Phi}^\sigma = (\tilde{\phi}_e^\sigma)$  be the flow with components  $\tilde{\phi}_e^\sigma = s_e \phi_e^\sigma$ . Multiplying Eq. S4 by  $s_e$  and using  $s_e V'(\phi) = V'(s_e \phi)$  gives

$$d\tilde{\phi}_e^\sigma = -\lambda V'(\tilde{\phi}_e^\sigma)dt - \mu \sum_{v \in \mathcal{V}} \sum_{f \in \mathcal{E}} D_{ve} D_{vf} \tilde{\phi}_f dt + \sqrt{2\beta^{-1}} dW_{\sigma(e),t},$$

where we have also used  $dW_t = -dW_t$  by symmetry of the process  $\mathbf{W}$ . In other words,  $\tilde{\Phi}^\sigma$  and  $\Phi$  obey identical stochastic differential equations, meaning that  $s_e \phi_e^\sigma$  and  $\phi_e$  obey identical waiting time distributions. However,  $\phi_e^\sigma$  and  $-\phi_e^\sigma$  also obey identical waiting time distributions, because, for every state  $\Phi_0$ , there is an identical probability state  $-\Phi_0$  by symmetry of  $H$ . Therefore, any edges  $e_1$  and  $e_2$  for which there exists  $\sigma \in \text{Aut}(\Gamma)$  with  $e_2 = \sigma(e_1)$  will have identical waiting time distributions.

Note that, in the incompressible limit  $\mu \rightarrow \infty$ , there may also be pairs of edges with identical waiting time distributions for which no such  $\sigma$  exists, even in connected simple graphs.

### SI Energy Barriers

We describe here the process of computing the transition energy barriers for  $K_4$  in the limit  $\mu/\lambda \gg 1$ . We assume incompressibility throughout the transition, and enforce this by directly solving the

constraints, although a cycle basis would yield the same result. Using the vertex labelings and edge orientations in Fig. 1A, let  $\phi_1$ ,  $\phi_2$ , and  $\phi_3$  be the flows on the outer edges  $2 \rightarrow 3$ ,  $2 \rightarrow 4$ , and  $3 \rightarrow 4$ , respectively. Then the flows on the other three edges are fixed by the four vertex constraints (one of which is redundant), giving energy  $H(\phi_1, \phi_2, \phi_3) = \lambda \mathcal{H}(\phi_1, \phi_2, \phi_3)$ , where

$$\mathcal{H}(\phi_1, \phi_2, \phi_3) = V(\phi_1) + V(\phi_2) + V(\phi_3) + V(\phi_1 + \phi_2) + V(\phi_2 + \phi_3) + V(\phi_3 - \phi_1).$$

Extrema of  $\mathcal{H}$  can then be evaluated numerically. By symmetry, we need only consider one particular transition. Let  $\Phi_a$  be the state with unit flux on the 3-cycle  $1 \rightarrow 2 \rightarrow 3 \rightarrow 1$  where  $(\phi_1, \phi_2, \phi_3) = (1, 0, 0)$ . Similarly, let  $\Phi_c$  be the 4-cycle  $1 \rightarrow 2 \rightarrow 3 \rightarrow 4 \rightarrow 1$  where  $(\phi_1, \phi_2, \phi_3) = (1, 0, 1)$ . These are separated by a saddle point  $\Phi_b$  with  $(\phi_1, \phi_2, \phi_3) \approx (1.03, 0, 0.44)$ , where  $\mathcal{H}(\Phi_b) \approx -0.20$ . Because  $\mathcal{H}(\Phi_a) = -1/4$  and  $\mathcal{H}(\Phi_c) = -1/3$ , this gives transition energy barriers  $\Delta H_{ab} \approx 0.45\lambda$  from a 3- to a 4-cycle and  $\Delta H_{cb} \approx 0.54\lambda$  from a 4- to a 3-cycle.

Note that the transition is not exactly of the form  $(\phi_1, \phi_2, \phi_3) = (1, 0, s)$  with  $0 \leq s \leq 1$ , as it would be were it only adding or removing a unit of flux around a 3-cycle. Instead, the saddle point is slightly displaced from  $\phi_1 = 1$ . However, this effect is small, and  $\phi_2$  remains at  $\phi_2 = 0$  throughout.

### SI Incompressible Limit

**Dimensional Reduction.** Let  $\mathbf{L} = \mathbf{D}^T \mathbf{D}$  be the ( $|\mathcal{E}| \times |\mathcal{E}|$ , symmetric, positive semidefinite) Laplacian matrix on edges, and let  $\{\Psi^1, \Psi^2, \dots, \Psi^{|\mathcal{E}|}\}$  be an orthonormal basis of eigenvectors of  $\mathbf{L}$  with components  $\Psi^i = (\psi_e^i)$  and corresponding real, nonnegative eigenvalues  $\{\nu_1, \nu_2, \dots, \nu_{|\mathcal{E}|}\}$ . Now, using summation convention, let  $f_i = \phi_e \psi_e^i$  be the components of  $\Phi$  in this basis. Then, by orthonormality of the basis vectors,  $\phi_e = f_j \psi_e^j$ , so  $f_i$  obeys

$$df_i = -\lambda V'(f_j \psi_e^j) \psi_e^i dt - \mu \nu_i f_i dt + \sqrt{2\beta^{-1}} \psi_e^i dW_{e,t},$$

with no sum over  $i$ . As  $\mu \rightarrow \infty$ , the second term damps to zero all  $f_i$  with nonzero eigenvalues  $\nu_i > 0$ , leaving only components with  $\nu_i = 0$ . The corresponding eigenvectors span  $\ker \mathbf{D}$ , the space of all incompressible flows termed the cycle space or flow space. Furthermore, orthonormality implies the noise term  $\psi_e^i dW_{e,t}$  reduces to a single term of unit variance. Therefore, in this limit, the system obeys

$$df_\alpha = -\frac{\partial \hat{H}}{\partial f_\alpha} dt + \sqrt{2\beta^{-1}} dW_{\alpha,t},$$

where Greek indices run over only those components where  $\nu_\alpha = 0$ , and we use the reduced energy

$$\hat{H} = \lambda \sum_{e \in \mathcal{E}} V(f_\alpha \psi_e^\alpha).$$

Having reduced the dynamics onto  $\ker \mathbf{D}$ , we are now free to change basis inside this subspace. In general, the orthonormal basis  $\{\Psi^\alpha\}$  will not be physically intuitive, because its basis vectors include fractional flows on many edges. More comprehensible is a cycle basis, where basis vectors comprise unit flux flows around closed cycles. Such a basis of  $\ker \mathbf{D}$  always exists, although this intuitiveness comes at the cost of nonorthogonality. Nevertheless, a cycle basis is particularly effective for planar graphs, as we describe in *Incompressible Limit*.

**Cycle Basis for  $P_{4,1}$ .** We detail here the derivation of the planar cycle basis representation in the incompressible limit for the cube  $P_{4,1}$ .

Using the embedding shown in Fig. S2A, orient and number the edges as indicated. Next, construct the dual of the (undirected) plane graph, with vertices numbered as in Fig. S2B, and assign an orientation to each edge of the dual such that  $A \rightarrow B$  implies that the flow on the edge between faces  $A$  and  $B$  is  $F_B - F_A$ , where  $F_\alpha$  is the flow anticlockwise around face  $\alpha$  (Fig. S2B). This has incidence matrix

$$\mathbf{I} = \begin{pmatrix} -1 & 0 & 0 & 0 & -1 & 0 & 0 & 1 & 1 & 0 & 0 & 0 \\ 0 & 1 & 0 & 0 & 1 & -1 & 0 & 0 & 0 & -1 & 0 & 0 \\ 0 & 0 & 1 & 0 & 0 & 1 & -1 & 0 & 0 & 0 & -1 & 0 \\ 0 & 0 & 0 & 1 & 0 & 0 & 1 & -1 & 0 & 0 & 0 & -1 \\ 1 & -1 & -1 & -1 & 0 & 0 & 0 & 0 & 0 & 0 & 0 & 0 \\ 0 & 0 & 0 & 0 & 0 & 0 & 0 & 0 & -1 & 1 & 1 & 1 \end{pmatrix},$$

the rows of which are the cycle basis vectors. General face flow components  $\mathbf{F} = (F_1, \dots, F_6)$  then translate to edge flows  $\Phi = (\phi_1, \dots, \phi_{12})$  as  $\phi_e = F_\alpha I_{\alpha e}$ . However, there is a degree of freedom: adding a constant to each component of  $\mathbf{F}$  results in the same  $\Phi$ , so, to obtain a unique correspondence between  $\mathbf{F}$  and  $\Phi$ , we fix the external face flux  $F_6 = 0$ . Let  $\mathbf{A}$  be  $\mathbf{I}$  with the corresponding final row omitted and drop the final component of  $\mathbf{F}$ . Then, for  $\Phi \in \ker \mathbf{D}$ ,  $\phi_e = F_\alpha A_{\alpha e}$  inverts to  $F_\alpha = P_{\alpha e} \phi_e$  with  $\mathbf{P} = (\mathbf{A}\mathbf{A}^T)^{-1}\mathbf{A}$ . Thus, the truncated dual Kirchhoff matrix  $\tilde{\mathbf{L}} = \mathbf{A}\mathbf{A}^T$ —which is independent of the edge orientations in Fig. S2B—reads

$$\tilde{\mathbf{L}} = \begin{pmatrix} 4 & -1 & 0 & -1 & -1 \\ -1 & 4 & -1 & 0 & -1 \\ 0 & -1 & 4 & -1 & -1 \\ -1 & 0 & -1 & 4 & -1 \\ -1 & -1 & -1 & -1 & 4 \end{pmatrix},$$

giving a noise covariance  $\mathbf{P}\mathbf{P}^T = \tilde{\mathbf{L}}^{-1}$  in Eq. 6 reading

$$\tilde{\mathbf{L}}^{-1} = \frac{1}{24} \begin{pmatrix} 10 & 5 & 4 & 5 & 6 \\ 5 & 10 & 5 & 4 & 6 \\ 4 & 5 & 10 & 5 & 6 \\ 5 & 4 & 5 & 10 & 6 \\ 6 & 6 & 6 & 6 & 12 \end{pmatrix}.$$

Observe that nonadjacent face pairs such as faces 1 and 3 have correlated noise.

## SI Complex Networks

Finally, we elaborate on discussions in the main text extrapolating our results to expected behavior on large complex networks.

Unlike the cubic graphs we have focused on, a complex network possesses a broad vertex degree distribution. This will certainly affect transition rates, because the presence of even-degree vertices deepens energy minima (Fig. S1). However, because the effect of vertex degree is broadly independent of cycle structure, we predict that the distribution of transition rates will still qualitatively match the  $e$ -girth distribution. In Fig. S3, we plot  $e$ -girth distributions derived from 10 instances each of four random graph distributions on 1,000 vertices: fixed degree 3, uniform, Barabási–Albert (“scale free”), and Watts–Strogatz (“small world”). Of the four, random cubic graphs display by far the highest  $e$ -girths, whereas the Barabási–Albert and Watts–Strogatz graphs, commonly used as prototypes of certain forms of real-life complex networks, both retain many edges with low  $e$ -girth despite their size. Therefore, by this measure, complex networks may exhibit a far greater proportion of fast-switching edges than random cubic graphs on the same number of vertices.

## SI Numerical Methods

**Numerical Integration and Waiting Times.** Eqs. 2 and 6 were integrated by the Euler–Maruyama method with time step  $\delta t = 5 \times 10^{-3}$ . After an initialization period to  $t = 500$ , state transition waiting times in Figs. 1–3 were determined by applying a moving average filter of width  $\Delta t \approx 3$  to eliminate noise-induced recrossings of  $\pm 1/2$  without a true state change, rounding to the nearest integer, and computing the times between changes in this integer state. Waiting times were aggregated over sets of 16 integrations to  $t = 4 \times 10^9$  for each  $\lambda$  in Fig. 1, and over 24 (Fig. 2) or 8 (Fig. 3) integrations to  $t = 1.6 \times 10^6$  for each graph in Figs. 2 and 3.

**Graph Generation and Properties.** Mathematica (Wolfram Research, Inc.) was used to generate graphs and their incidence matrices, and to determine all graph-theoretic properties, including cycle lengths and edge equivalence classes. The graphs in Fig. 3 (see also Fig. S4) were chosen uniformly at random from the database of all non-isomorphic bridgeless connected cubic graphs on 14 vertices accessible in Mathematica after filtering to discard those with nontrivial automorphism group.



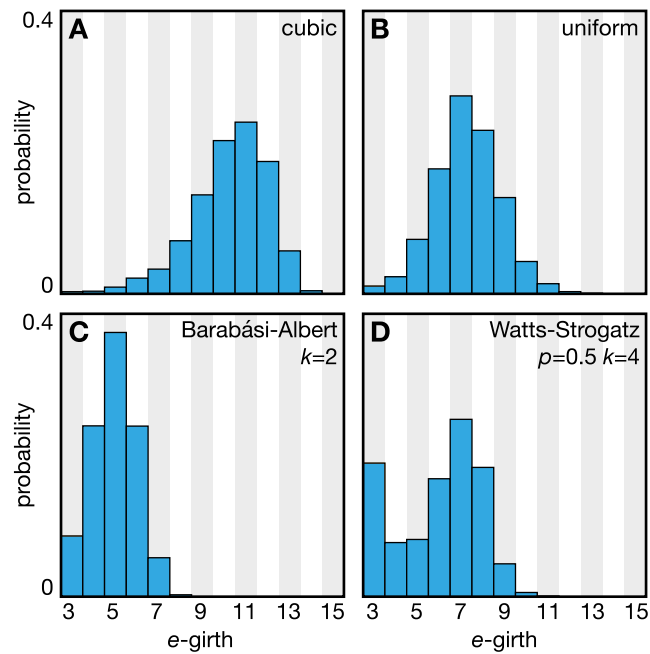


**Fig. S3.** Empirical probability distributions of e-girth determined from 10 graph realizations each from four random 1,000-vertex graph ensembles: (A) fixed degree 3, i.e., cubic; (B) uniform with 1,500 edges; (C) scale-free Barabási–Albert with a degree  $k=2$  vertex added at every step; and (D) small-world Watts–Strogatz with rewiring probability  $p=0.5$  and mean degree  $k=4$ . The pseudo-real-life networks of C and D exhibit distributions with far more small e-girth edges than the more generic random graphs in A and B.

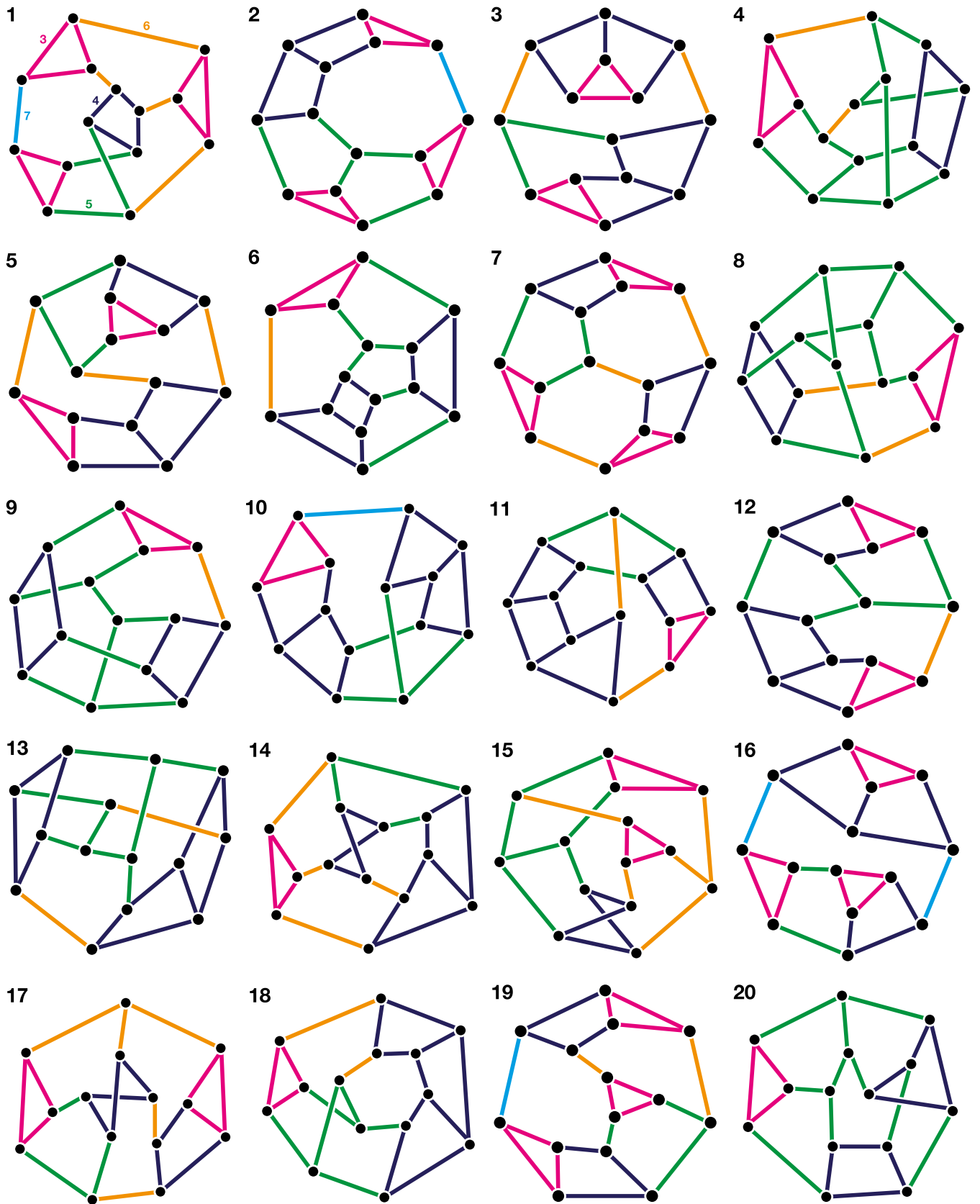
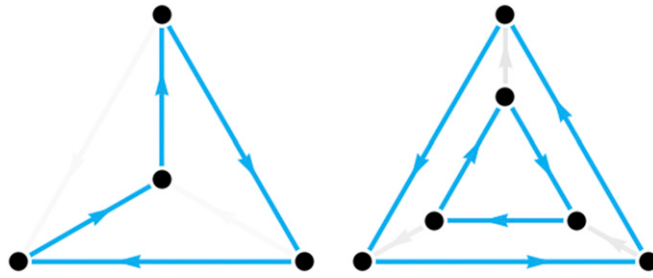


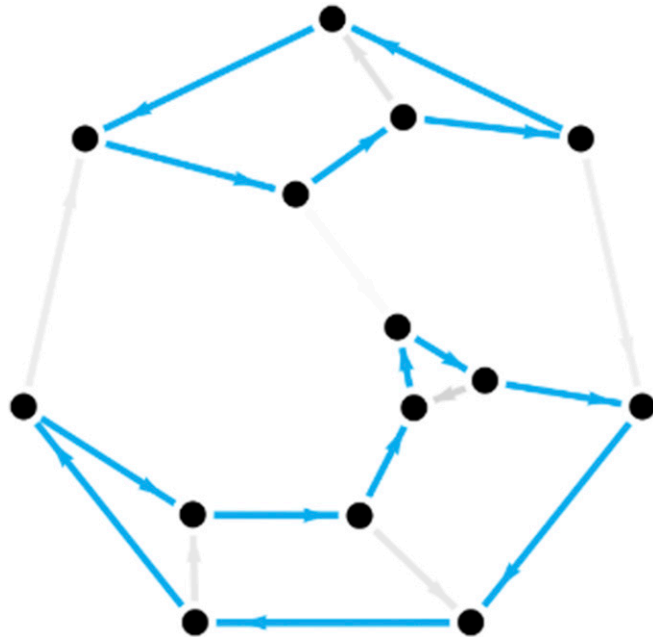
**Fig. 54.** The 20 nonisomorphic asymmetric cubic graphs in Fig. 3. Edges are colored according to e-girth as indicated in graph 1 and in Fig. 3. Graph 19 is that illustrated in Fig. 3B. All planar graphs (graphs 2, 3, 5, 6, 7, 12, 16, and 19) are shown in a planar embedding.





**Movie S1.** Stochastic cycle selection in the graphs  $K_4$  (Left) and  $P_{3,1}$  (Right). Each graph shows an integration of the active network model up to  $t = 2 \times 10^4$ , played back such that 1 s is  $\Delta t = 900$ . Flowing edges above  $|\phi_e| > 1/2$  are cyan, nonflowing edges fluctuate from white at  $|\phi_e| = 0$  to gray at  $|\phi_e| = 1/2$ . Parameters are  $\lambda = 2.5$ ,  $\mu = 25$ , and  $\beta^{-1} = 0.05$ .

[Movie S1](#)



**Movie S2.** Stochastic cycle selection in an asymmetric bridgeless cubic graph on 21 edges. The graph shows an integration of the active network model on the graph shown in Fig. 3B (graph 19 of Fig. S4) up to  $t = 1.6 \times 10^6$ , played back such that 1 s is  $\Delta t = 72,000$ . Flowing edges above  $|\phi_e| > 1/2$  are cyan, nonflowing edges fluctuate from white at  $|\phi_e| = 0$  to gray at  $|\phi_e| = 1/2$ . Parameters are  $\lambda = 2.5$ ,  $\mu = 25$ , and  $\beta^{-1} = 0.05$ .

[Movie S2](#)